Production of ethanol fuel via syngas fermentation

Optimization of economic performance and energy efficiency

de Medeiros, Elisa M.; Noorman, Henk; Maciel Filho, Rubens; Posada, John A.

DOI
10.1016/j.cesx.2020.100056

Publication date
2020

Document Version
Final published version

Published in
Chemical Engineering Science: X

Chemical Engineering Science: X xxx (xxxx) xxx

Contents lists available at ScienceDirect

Chemical Engineering Science: X

journal homepage: www.elsevier.com/locate/cesx

Production of ethanol fuel via syngas fermentation: Optimization of economic performance and energy efficiency

Elisa M. de Medeiros [a,b,*], Henk Noorman [a,c], Rubens Maciel Filho [b], John A. Posada [a]

[a] Department of Biotechnology, Delft University of Technology, van der Maasweg 9, Delft 2629 ZH, the Netherlands
[b] School of Chemical Engineering, University of Campinas, Av. Albert Einstein 500, Campinas 13084-852, Brazil
[c] DSM Biotechnology Center, PO Box 1, Delft 2600 MA, the Netherlands

ARTICLE INFO

Article history:
Received 13 September 2019
Received in revised form 16 January 2020
Accepted 21 January 2020
Available online xxxx

Keywords:
Bioethanol production
Renewable energy
Modeling
Multi-objective optimization
Syngas fermentation
Artificial neural networks

ABSTRACT

In this work, a model was developed to predict the performance of a bubble column reactor for syngas fermentation and the subsequent recovery of anhydrous ethanol. The model was embedded in an optimization framework which employs surrogate models (artificial neural networks) and multi-objective genetic algorithm to optimize different process conditions and design variables with objectives related to investment, minimum selling price, energy efficiency and bioreactor productivity. The results indicate the optimal trade-offs between these objectives while providing a range of solutions such that, if desired, a single solution can be picked, depending on the priority conferred to different process targets. The Pareto-optimal values of the decision variables were discussed for different case studies with and without the recovery unit. It was shown that enhancing the gas-liquid mass transfer coefficient is a key strategy toward sustainability improvement.

1. Introduction

Biofuels are one of the possible means to reduce CO_2 emissions in transportation, a sector responsible for roughly 25% of global greenhouse gas (GHG) emissions in 2016 (IEA, 2019). However, the rapid expansion of 1st generation biofuels (i.e. those produced from food crops) has also been associated with impacts that were initially neglected or unforeseen, such as deforestation, indirect land use change, and significant GHG emissions during agricultural stages (Goldemberg et al., 2008). Lignocellulosic or 2nd generation biofuels have the potential to minimize these impacts by using waste carbon materials such as agricultural residues, forestry waste and marginal land (energy) crops. Yet, despite large efforts towards commercialization, most of these production pathways face technical challenges that are inherent to emerging technologies. An alternative path to biofuels and the object of this work is syngas fermentation, the microbial conversion of $CO/H_2/CO_2$ to ethanol and potentially other chemicals using facultative autotrophic bacteria called acetogens. Since syngas can be produced via gasification of multiple types of feedstocks – including even municipal solid waste –, this process is considered a promising and flexible alternative to biochemical routes that rely on the liberation of sugars from lignocellulosic biomass. Moreover, it also constitutes a valorization pathway for works arising gases (WAG) from steel production containing large amounts of CO, as demonstrated by the increasing number of commercial projects led by LanzaTech and partners in the past years (ArcelorMittal, 2019; Biofuels Digest, 2019; Renewables Now, 2018).

In order to upgrade the technology readiness level (TRL) and achieve full commercialization, not only scaling-up technical issues need to be resolved, but the process also needs to be boosted at different levels, for example: improving gas-liquid mass transfer through better reactor design; genetically engineering bacteria; adjusting the gasification process to deliver syngas with favorable composition; reducing energy use in the product recovery unit; and tuning the process conditions at all units simultaneously to approach overall optimal operation. Most published research about syngas fermentation has focused on running experiments to test the capabilities of different strains and reactor configurations, and to study the effects of changing nutritional composition of the liquid medium as well as the pH, such as done by Abubackar et al. (2015). Many studies have also tried to elucidate the metabolism of these microbes so that yield and selectivity of the desired product (usually ethanol) can be improved (Richter et al., 2016). On the other hand, studies about modeling, simulation and optimization are still limited, despite being of paramount importance for the evaluation of feasibility and comprehension of these systems. A few recent works have discussed results obtained with simulations using Aspen plus, such as de Medeiros et al. (2017),

* Corresponding author.
E-mail address: E.MagalhaesdeMedeiros@tudelft.nl (E.M. de Medeiros).

https://doi.org/10.1016/j.cesx.2020.100056
2590-1400/

Nomenclature

Greek symbols

γ	liquid phase activity coefficient
ε_G	gas hold-up
η	thermodynamic efficiency
μ	biomass growth rate [h^{-1}]
ν_i	consumption or production rate of component i [$mol \cdot g^{-1} \cdot h^{-1}$]
ρ_L	mass density of liquid [$kg \cdot m^{-3}$]

Roman symbols

a	bubble column operation mode (1 for concurrent, −1 countercurrent)
AE	anhydrous ethanol
ANN	artificial neural network
AR	vessel aspect ratio (BCR)
BCR	bubble column reactor
$C_{G,i}$, $C_{L,i}$	concentration of component i (gas or liquid phase) [$mol \cdot m^{-3}$ or $g \cdot L^{-1}$]
$C^*_{G,i}$, $C^*_{L,i}$	Saturation concentration of component i (gas or liquid phase) [$mol \cdot m^{-3}$]
$C_{L,X}$	concentration of cells in the broth [$g \cdot L^{-1}$]
C_{OL}, C_{RM}, C_{UT}, C_{WT}	costs of operating labor, raw materials, utilities and waste treatment [$/year]
C_{BM}, C_{TM}	mare module cost, total module cost [$]
COM_d	manufacturing costs excluding depreciation costs
C_p^0	purchase cost of equipment at base conditions
d_C	vessel diameter (BCR) [m]
D:F	mass ratio distillate stream to feed stream
Df_i	diffusivity coefficient of component i in water [$cm^2 \cdot s^{-1}$]
D_L	axial dispersion coefficient [$m^2 \cdot h^{-1}$]
D_{rate}	dilution rate in the BCR [h^{-1}]
DV	decision variable
EtOH	ethanol
F_{BM}	bare module cost factor
F_{ST}	feed stage (T-01 or T-02)
GRR	gas recycle ratio (BCR)
GRT	gas residence time at the bottom of the reactor [min]
H_i	Henry's law constant of component i in water [Pa]
HAc	acetic acid
HMT	high mass transfer (case study)
k_d	cell death rate [h^{-1}]
k_La	volumetric mass transfer coefficient [h^{-1}]
K_T	temperature adjustment coefficient for k_La
L	length of vessel (BCR) [m]
LHV	lower heating value [$MJ \cdot kg^{-1}$ or $MJ \cdot kmol^{-1}$]
$\dot{m}$	mass flow rate [$kg \cdot h^{-1}$ or $kg \cdot year^{-1}$]
MESP	minimum ethanol selling price [$\$ \cdot L^{-1}$]
MML	million liters
MM_L	molar mass liquid phase [$g \cdot mol^{-1}$]
MOGA	multi-objective genetic algorithm
$\dot{n}_{MT}$	mass transfer rate [$mol \cdot m^{-3} \cdot h^{-1}$]
N_{ST}	number of stages (T-01 or T-02)
OF	objective function
$P_{sat,i}$	vapor pressure of component i [Pa]
Q_G, Q_L	volumetric flow rate of gas or liquid in the BCR [$m^3 \cdot h^{-1}$]
R	gas constant = 8.314 $J \cdot mol^{-1} \cdot K^{-1}$
RR	molar reflux ratio (T-01 or T-02)
S:F	mass ratio side stream to feed stream
T	temperature [°C or K]
u_G, u_L	gas or liquid superficial velocity [$m \cdot h^{-1}$]
V_L	volume of liquid (BCR) [m^3]
V_R	volume of reactor vessel (BCR) [m^3]
X_i	gas conversion (BCR), i = CO, H_2
XP	cell purge fraction (BCR)

Benalcázar et al. (2017), Pardo-Planas et al. (2017) and Roy et al. (2015). Though these studies look at the whole process from feedstock (biomass) to ethanol and provide meaningful estimates of process performance in different domains (technical, economic and environmental), the process conditions were mostly fixed or in some cases changed through univariate sensitivity analysis, and simulation of the bioreactor was based on strong assumptions and simplifications with limited connection to the operating conditions. In a previous study (de Medeiros et al., 2019), we discussed the contributions of more elaborate bioreactor models developed by other authors and presented the model of a dynamic continuous stirred tank (CSTR), demonstrating its application for sensitivity analysis and technical optimization. In the present work, we extended the CSTR model to a bubble column reactor model (BCR) with distribution of key process variables in time and space, and employed it in the optimization of operating (e.g. dilution rate) and design (e.g. reactor size) variables considering different objectives in parallel, both technical and economic. The BCR model was first considered standalone and subsequently integrated with the distillation unit, whose input was concurrently optimized. The contributions of this paper can be summarized as follows:

(i) Development of a spatial dynamic model of a bubble column reactor (BCR) for syngas fermentation considering kinetics of cell growth and death, mixed product formation and acetic acid re-assimilation.
(ii) Application of artificial neural networks as surrogate models for two types of intricate models: BCR model and distillation model (nonlinear system of MESH equations – material-equi librium-summation-enthalpy – solved in Aspen Plus).
(iii) Development of a multi-objective optimization framework for the integrated process of anhydrous ethanol production from syngas via fermentation and distillation.
(iv) Evaluation of Pareto-optimal solutions for the most important input variables of the system, in terms of economic performance, thermodynamic efficiency and productivity.

2. Methodology

2.1. Process overview

Fig. 1 presents the conceptual process flowsheet to produce anhydrous ethanol from syngas, which consists of three main unit operations: (i) the syngas bioreactor (R-01); ethanol distillation (T-01 and T-02) to achieve azeotropic composition (also called hydrous ethanol); (iii) ethanol dehydration in molecular sieves (T-04 and T-05) to achieve 99.5% ethanol. There is also a vent scrubber (T-03) to recover any ethanol present in CO_2 off-gases. Three main types of stream are recycled to the bioreactor: (i) water from the distillation bottoms and the scrubber; (ii) unconverted syngas; and (iii) microbial cells. Sections 2.2 and 2.3 lay out the methodology for process design and modeling of the two main blocks of the process: fermentation and product recovery.

2.2. Model of syngas fermentation in bubble column reactor (BCR)

The syngas bioreactor consists of a bubble column where syngas enters at the bottom and off-gas leaves from the top, a fraction of it being recycled back to the bottom after compression and cooling. Liquid flows continually in and out of the reactor and a fraction

Please cite this article as: E. M. de Medeiros, H. Noorman, R. Maciel Filho et al., Production of ethanol fuel via syngas fermentation: Optimization of economic performance and energy efficiency, Chemical Engineering Science: X, https://doi.org/10.1016/j.cesx.2020.100056

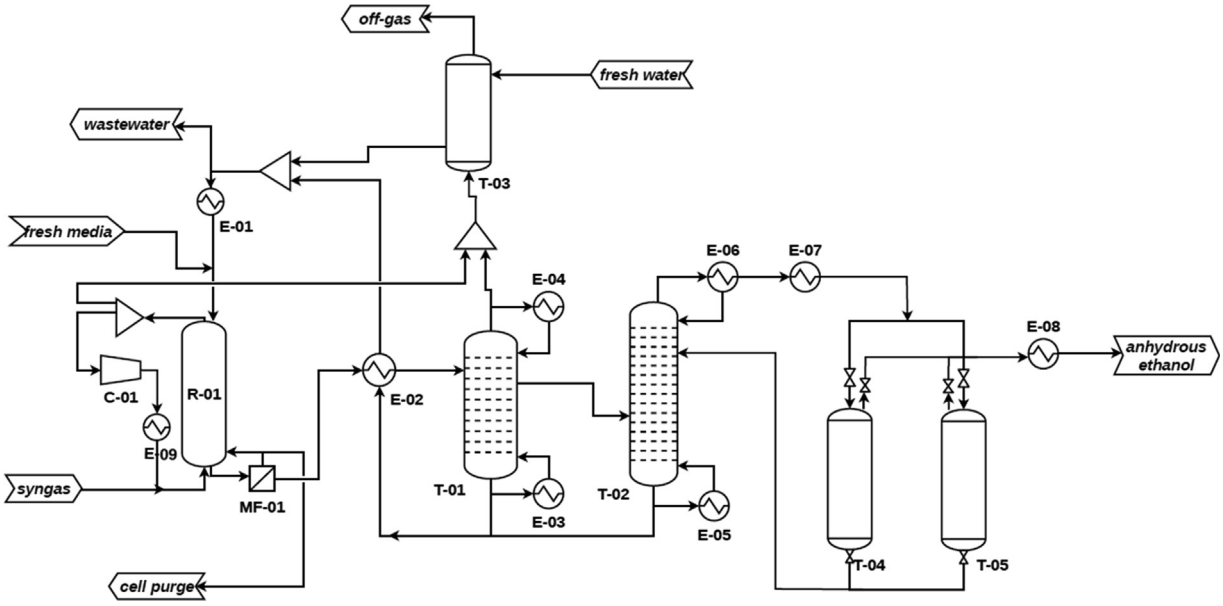

Fig. 1. Simplified PFD of anhydrous ethanol production from syngas. C-01: gas compressor; E-01 to E-09: heat exchangers; MF-01: microfiltration membrane; R-01: syngas bubble column reactor; T-01 and T-02: distillation columns; T-03: vent scrubber; T-04 and T-05: adsorption and regeneration columns.

of bacterial cells are recycled after separation from the products in a microfiltration membrane. In the reactor, cells are dispersed in the liquid phase, where they consume CO, H_2 and CO_2 and produce ethanol, acetic acid and CO_2. The latter is both a product from the oxidation of CO and a source of carbon in the reaction with H_2, therefore its consumption or production rate will depend on the availability of the other two molecules.

Similar models for this process with spatiotemporal distribution have been presented by Chen et al. (2018) and Li et al. (2019), the main difference being the method to calculate the consumption/production rates of components which in their works was done via Flux Balance Analysis (FBA) while in the present study we employ the microbial kinetics developed in our previous work (de Medeiros et al., 2019). Moreover, the procedure to estimate the gas velocity profile and hydrodynamic parameters (assumed constant by Chen et al. (2018)) is different. FBA is a powerful tool for the comprehension of cell metabolism, enabling for example *in silico* simulations about the effects of gene deletion and knockout; however, it also adds a significant amount of complexity to the model with the inclusion of a linear programming problem that must be solved during the integration of the ODEs. Furthermore it requires the definition of an objective function (e.g. maximizing the biomass growth rate) and flux bounds which are not always known and might not be constant during the process. The kinetic model used in this work, on the other hand, is based on global reactions for the consumption of gases and formation of products, embedding parameters that were previously estimated with experimental data.

The BCR was described here with the axial dispersion model of Deckwer (1992), considering the following assumptions: (i) isothermal operation at T = 37 °C; (ii) axial dispersion considered in the liquid phase but neglected in the gas phase; (iii) the pressure profile is calculated from the liquid head; (iv) biochemical reactions occur in the liquid phase with rates depending on the concentrations of the components; (v) gas velocity changes along the column as the gas shrinks due to microbial conversion or expands due to pressure reduction; (vi) hydrodynamic parameters are a function of the gas superficial velocity assuming heterogeneous flow in air-water systems. In total 13 state variables are distributed in space: the concentrations [mol·m^{-3}] of six chemical species in the gas and in the liquid, i.e. $C_{G,i}$ and $C_{L,i}$ where $i = CO, H_2, CO_2$, ethanol ($EtOH$), acid acid (HAc), and H_2O; and the concentration of cells in the liquid $C_{L,X}$ [g·m^{-3}]. Eqs. (1)–(3) summarize the governing partial differential equations (PDEs) which are completed by the algebraic equations for the calculation of mass transfer rates (Eq. (4)) and cell kinetics. For the latter, the variables v_i (production/-consumption rates), μ (cell growth rate) and k_d (cell death rate) are calculated or specified as explained in de Medeiros et al. (2019), at each discrete point of the system. The physical properties H_i, $P_{sat,i}$ and γ_i can also be found in de Medeiros et al. (2019). In Eqs. (2) and (3), $a = 1$ if the column is operating concurrently and $a = -1$ otherwise. For the optimizations in the present work, the latter is adopted.

$$\frac{\partial C_{G,i}}{\partial t} = -\frac{u_G}{\varepsilon_G}\cdot\frac{\partial C_{G,i}}{\partial x} - \frac{C_{G,i}}{\varepsilon_G}\cdot\frac{\partial u_G}{\partial x} - \frac{\dot{n}_{MT}}{\varepsilon_G} \tag{1}$$

$$\frac{\partial C_{L,i}}{\partial t} = -\frac{a u_L}{(1-\varepsilon_G)}\cdot\frac{\partial C_{L,i}}{\partial x} + D_L\frac{\partial^2 C_{L,i}}{\partial x^2} + \frac{\dot{n}_{MT}}{(1-\varepsilon_G)} + v_i C_{L,X} \tag{2}$$

$$\frac{\partial C_{L,X}}{\partial t} = -\frac{a u_L}{(1-\varepsilon_G)}\cdot\frac{\partial C_{L,i}}{\partial x} + D_L\frac{\partial^2 C_{L,i}}{\partial x^2} + (\mu - k_d)C_{L,X} \tag{3}$$

$$\dot{n}_{MT} = k_L a_i\left(C^*_{L,i} - C_{L,i}\right)\ ,\ C^*_{L,i} = \frac{C_{G,i}}{m_i}\ ,\ m_i = \frac{H_i\cdot MM_L}{R\cdot T\cdot \rho_L}\ ,\ i = CO, H_2, CO_2 \tag{4a}$$

$$\dot{n}_{MT} = -k_L a_i\left(C^*_{G,i} - C_{G,i}\right)\ ,\ C^*_{G,i} = \frac{C_{L,i}}{m_i}\ ,\ m_i = \frac{\rho_L\cdot R\cdot T}{MM_L\cdot\gamma_i\cdot P_{sat,i}}\ i = EtOH, HAc, H_2O \tag{4b}$$

The gas hold-up ε_G and the volumetric mass transfer coefficient k_La [h^{-1}] were calculated from the correlations by Heijnen and van't Riet (1984), adapted in Eqs. (5) and (6), where u_G [m·h^{-1}] is the gas superficial velocity. In Eq. (6), the first term between brackets is the k_La for air in water at 20 °C, which is adjusted to component i using the diffusivity coefficient Df_i, and to the reactor temperature by means of the coefficient $K_T = (1.024)^{(T-20)} = 1.5$

Please cite this article as: E. M. de Medeiros, H. Noorman, R. Maciel Filho et al., Production of ethanol fuel via syngas fermentation: Optimization of economic performance and energy efficiency, Chemical Engineering Science: X, https://doi.org/10.1016/j.cesx.2020.100056

(Heijnen and van't Riet, 1984). The axial dispersion coefficient D_L [$m^2 \cdot h^{-1}$] (Eq. (7)) is calculated with the correlation provided by Deckwer et al. (1974).

$$\varepsilon_G = 0.6(u_G/3600)^{0.7} \tag{5}$$

$$k_L a = \left[(3600)\left(0.32 \cdot (u_G/3600)^{0.7}\right)\right] \cdot \left(Df_i/Df_{O_2,air}\right)^{1/2} \cdot K_T \tag{6}$$

$$D_L = (0.36)\left(2.7 \cdot (d_C \cdot 100)^{1.4} \cdot (u_G/36)^{0.3}\right) \tag{7}$$

Finite differences were used to transform the system of partial differential algebraic equations (PDAE) to a system of ordinary differential algebraic equations (DAE). This stiff problem was solved in MATLAB R2015b using *ode15s*, which is usually the first recommended option before trying other stiff solvers such as *ode23s*. The state vector contained thus 13•N variables where N = 15 is the number of discretization points. The boundary conditions for both phases at the bottom (x = 0) and at the top (x = L), considering counter-current operation, are shown in Eqs. (8) and (9).

$$C_{G,i}\big|_{x=0} - C_{G,i}^{in} = 0 \;,\; \left.\frac{\partial C_{L,i}}{\partial x}\right|_{x=0} = 0 \tag{8}$$

$$\left.\frac{\partial (C_{G,i} \cdot u_G)}{\partial x}\right|_{x=L} = 0 \;,\; C_{L,i}\big|_{x=L} - C_{L,i}^{in} + \frac{(1-\varepsilon_G)D_L}{u_L} \cdot \left.\frac{\partial C_{L,i}}{\partial x}\right|_{x=L} = 0 \tag{9}$$

The gas velocity u_G was calculated along the reactor by applying a mole balance in the gas phase of each compartment starting from the bottom. If the gas recycle ratio (*GRR*) is greater than zero (where GRR is the ratio between the gas flow rate recycled to the bottom of the bioreactor and the total gas flow rate at the top), then the flow rate and composition of the inlet are different from those of the fresh syngas. In these cases an iterative procedure was applied to find the correct properties of the inlet stream and the gas velocity profile: first an initial guess is assumed at the bottom and used for the calculation of the velocity along the column, the new properties calculated at the top are then used to recalculate the properties at the bottom, which replace the initial guess in the next iteration; the velocity profile is calculated again and this procedure is repeated until the differences are negligible between two consecutive iterations. Though this subroutine makes the model more intricate, neglecting the change in gas velocity is an unrealistic assumption (Deckwer, 1976) and substantial differences (>50%) between the velocity at the inlet and outlet have been observed not only with the model developed here but also by Li et al. (2018).

2.3. Product recovery unit

Anhydrous ethanol is recovered using distillation and molecular sieve adsorption. In the present work, the design of these operations was based on the flowsheet described by Humbird et al. (2011) for purification of ethanol produced via 2nd-generation biochemical route (dilute-acid pretreatment and enzymatic hydrolysis). First, the dilute broth (1–4% w/w ethanol) is fed to a beer column (T-01), from which water is removed at the bottom and CO_2 at the top, while concentrated ethanol is removed as a vapor-side stream and fed to the rectification column (T-02). The design choices adopted by Humbird et al. (2011) were considered as starting point and a preliminary analysis was done to evaluate the effects of different parameters (results not shown here). In the first column it was observed that the mass ratio of side stream to feed stream (S:F) had significantly stronger effects on the outcome (reboiler duty, ethanol recovery and concentration) than other parameters, therefore this was chosen as the only decision variable in this column. The other parameters were fixed in accordance with the abovementioned design, though with minor modifications: 25 stages, feed stream on the 5th stage from the top, vapor-side stream removed from the 7th stage, top pressure of 2 bar, and molar reflux ratio (RR) of 3:1. Though in the design presented by Humbird et al. (2011) the fermentation broth had a higher ethanol concentration (5.4% w/w), increasing RR beyond 3:1, even for lower ethanol concentrations, was found to have marginal effects on the separation performance, especially if considering the increased reboiler duty. The mass flow rate of the top stream, which is rich in CO_2, was defined so as to ensure that most of the dissolved CO_2 is removed, therefore it was fixed at 1.1 times the mass flow rate of CO_2 present in the feed stream.

The hot bottom stream from T-01, which contains most of the acetic acid from the feed, is used to pre-heat the latter (in E-02), whereas the CO_2 stream, together with off-gas from the BCR, is fed to the vent scrubber (T-03) to recover any ethanol that is present in these streams. The outlet liquid stream from T-03 is then mixed with bottoms from both distillation columns and part of the resulting stream is recycled to the bioreactor while the rest is sent to wastewater treatment. The concentrated ethanol stream from T-01, which contains between 20 and 40% w/w depending on the case, is sent to the rectification column (T-02) where it is further concentrated to near-azeotropic composition (92.5% w/w). The only fixed parameter in T-02 is the pressure (atmospheric); all the other inputs are decision variables, as explained further in Section 2.5. The distillate from T-02 is removed as saturated vapor and superheated to 116 °C before being sent to dehydration with molecular sieves (columns T-04 and T-05). This unit was not modelled but instead the outcomes were fixed considering two output streams: (i) the product (anhydrous ethanol, 99.5% w/w) which is then cooled to 38 °C (E-08); and (ii) a low-purity ethanol stream (72% w/w) produced during the regeneration step, which is recycled back to the rectifier.

The distillation columns were simulated in Aspen plus using the RadFrac model which solves the system of MESH equations with the Inside-Out algorithm. Four components were considered: water, ethanol, acetic acid and CO_2. The property methods were: for the liquid phase, the activity coefficient model NRTL, due to the non-ideal ethanol-water mixture; and for the gas phase, Hayden-O'Connell equation-of-state with Henry's law, due to low pressure, presence of acetic acid which may cause vapor phase association, and presence of dissolved gases (CO_2).

2.4. Artificial neural network (ANN) surrogate models

Surrogate modeling techniques have been applied by many authors in the past years with the goal of reducing the complexity of computationally expensive models. Throughout this paper we refer to the latter as "rigorous" models, although they also incorporate some level of simplification (e.g. equilibrium equations in the calculation of distillation columns).

Recent works, such as Ibrahim et al. (2018) and Ye et al. (2019) have demonstrated the efficacy of this methodology for separation processes, specifically for distillation and adsorption. In the present work, ANNs were trained with input from the two types of models laid out in Sections 2.2 and 2.3: (i) the PDAE system describing the BCR; and (ii) the RadFrac models in Aspen plus describing the distillation columns. In both cases, multi-layer feedforward networks were trained with Bayesian regularization backpropagation using the ANN Toolbox in MATLAB R2015b. The networks contained one input layer, one output layer and two hidden layers, with the number of neurons per hidden layer being chosen after a few tests (in all cases between 5 and 25). For some responses, an ensemble of networks was used to reduce the error of a single network by averaging the predictions of the individual networks and removing outliers. For all trained ANNs the correlation coefficient (R value)

Please cite this article as: E. M. de Medeiros, H. Noorman, R. Maciel Filho et al., Production of ethanol fuel via syngas fermentation: Optimization of economic performance and energy efficiency, Chemical Engineering Science: X, https://doi.org/10.1016/j.cesx.2020.100056

between network output and original response was higher than 0.99.

2.4.1. Bubble column reactor ANNs

Data was generated with the BCR model by varying the input vector and exporting the steady-state responses obtained after integration of the ODE system over a sufficiently long time span. Around 2000 points were used to train the ANNs. The input vector comprises in total 12 variables which are needed to define the DAE system, though not all of them are used as decision variables in the optimization: (i) dilution rate (D_{rate}), defined as the liquid volumetric flow rate (Q_L) divided by the liquid volume (V_L) in the bioreactor; (ii) the volume of liquid divided by the gas volumetric flowrate at the bottom of the reactor ($V_L/Q_{g,bot}$) which we refer to here as gas residence time (GRT); (iii) gas recycle ratio (*GRR*) defined in Section 2.2; (iv) cell purge fraction (*XP*), which is the fraction of biomass cells that are not recycled to the bioreactor; (v) vessel length (*L*); (vi) vessel aspect ratio (*AR*); (vii) and (viii) concentrations of acetic acid and ethanol in the inlet liquid stream; (ix) to (xii) molar fractions of CO, H_2, CO_2 and H_2O in the fresh syngas (note: for the optimization studies the syngas composition was fixed at 50% CO and 50% H_2). It should be noted that although the liquid inlet composition (items vii and viii) is an input of the bioreactor, it is not an input of the integrated process (and even less a decision variable in the optimization), because it depends on the properties of the recycle streams from the distillation unit.

The input matrix was generated using Latin hypercube sampling (LHS) to ensure good coverage of the input domain, which considers realistic ranges of these variables (presented together with optimization results in Tables 1 and 2). ANNs were trained to predict ten responses that are needed in the calculation of the objective functions or as input for the distillation unit. These responses belong to five categories: (i) concentrations of ethanol, acetic acid, cell biomass and dissolved CO_2 at the liquid outlet; (ii) gas superficial velocities at the bottom and at the top; (iii) gas conversions of CO and H_2; (iv) pressure at the bottom (this response is not straightforward because it depends on the gas hold-up which is not fixed); (v) total cooling duty to keep the reactor isothermal.

2.4.2. Distillation columns

Data for the distillation columns was generated using Aspen plus and Aspen Simulation Workbook, which was used to launch the simulations automatically (roughly 2000 points for each column). The main aspects of the simulations were detailed in Section 2.3; and the following variables were considered inputs for the ANNs, some of them being outputs of the bioreactor and others being key parameters related to the design and operation of the distillation column: (i) inlet mass fractions of ethanol, acetic acid and CO_2; (ii) number of stages (N_{ST}); (iii) feed stages (F_{ST}); (iv) molar reflux ratio (*RR*); (v) mass ratio of side to feed stream (*S:F*), only for T-01; (vi) mass ratio of distillate to feed stream (*D:F*), only for T-02; (vii) pressure at the top; (viii) feed stream mass flow rate. It should be noted that N_{ST} and F_{ST} are continuous variables when provided to the ANNs and for their training, but they are transformed to integer values before running the Aspen simulations. F_{ST} is written as a fraction of the number of stages, such that F_{ST} = 0 when the feed stage is the first after the reboiler and F_{ST} = 1 when it is the last before the condenser.

The following outputs were considered: (i) mass fractions of ethanol and acetic acid at the bottom, at the top, and at the side stream (only for T-01); (ii) same for temperatures; (iii) column diameter; (iv) reboiler and condenser duties.

Multilayer feedforward neural networks were trained for both pattern recognition and function approximation. In the first case, the ANNs were trained to classify the input vector as feasible or infeasible according to the convergence status of the Aspen simulations. The results of the successful simulations were then used to train the ANNs as explained previously in Section 2.4.

2.5. Optimization framework

Multi-objective genetic algorithm (MOGA) was employed to first optimize the standalone BCR and later the integrated process, with regard to the following objectives: (i) in the BCR, maximization of ethanol productivity and minimization of *CAPEX*; and (ii) in the whole process (shown in Fig. 1), minimization of *CAPEX* per annual production of anhydrous ethanol ($\dot{m}_{AE}$), minimization of minimum ethanol selling price (*MESP*) and maximization of thermodynamic efficiency (η). MOGA aims at finding a set of non-dominated (i.e. optimal) solutions approaching the true Pareto front of the system, i.e. those feasible points for which one objective function can only be reduced if other objective functions are increased. It's worth noting that MOGA does not use weighted functions to transform multiple objectives into one, therefore it ensures that objectives of different natures are considered fairly. Though other methods exist for multi-objective optimization,

Table 1
Multi-objective optimization of the bubble column reactor: ranges of decision variables and process outcomes at the Pareto-optimal solutions.

	Search space	base	HMT
D_{rate} [h^{-1}]	0.01–0.15	0.088–0.14	0.11–0.15
GRT [min]	5–50	6.41–36.9	5.15–35.8
GRR	0–0.5	0.032–0.43	0.017–0.32
XP	0.05–0.2	0.035–0.049	0.025–0.056
L [m]	25–50	35.6–47.3	35.5–42.5
V_R [m^3]	500–900	502–572	500–548
$C_{L,EtOH}$ [$g{\cdot}L^{-1}$]	–	6.21–34.1	12.5–39.5
$C_{L,HAc}$ [$g{\cdot}L^{-1}$]	–	1.35–2.75	2.17–2.98
X_{CO}	–	0.56–0.74	0.81–0.93
X_{H_2}	–	0.42–0.66	0.56–0.87

Table 2
Multi-objective and single-objective optimization of the integrated process: ranges of decision variables at the Pareto-optimal or optimal solutions.

	Search space	*CAPEX* × η	*CAPEX* × η (HMT)	*MESP* × η	*MESP* × η (HMT)	*MESP*	*MESP* (HMT)
D_{rate} (BCR) [h^{-1}]	0.01–0.15	0.044–0.092	0.1022–0.1025	0.050–0.087	0.101–0.103	0.099	0.106
GRT (BCR) [min]	5–50	8.95–44.4	15.7–17.7	15.9–39.1	18.3–18.9	14.5	21.3
GRR (BCR)	0–0.5	0.062–0.43	0.489–0.493	0.092–0.45	0.478–0.496	0.0086	0.061
XP (BCR)	0.05–0.2	0.084–0.19	0.0553–0.0639	0.12–0.17	0.044–0.054	0.198	0.0902
L (BCR) [m]	25–50	44.9–49.9	41.3–43.4	48.3–49.9	42.6–42.8	49.9	47.2
V_R (BCR) [m^3]	500–900	710–853	630–645	713–811	645–654	633	595
S:F (T-01)	0.04–0.3	0.094–0.106	0.0796–0.0818	0.096–0.10	0.079–0.080	0.0963	0.0824
N_{ST} (T-02)	40–50	40–46	43–45	43–47	44	41	40
$F_{ST,V}$ (T-02)	0.6–0.9	0.62–0.76	0.755–0.773	0.61– 0.80	0.76–0.78	0.67	0.724
$F_{ST,L}$ (T-02)	0.2–0.5	0.26–0.47	0.336–0.359	0.297–0.496	0.34–0.36	0.22	0.456
RR (T-02)	3–6	4.4–5.80	3.78–3.89	5.14–5.83	3.95–4.02	5.25	4.17

Please cite this article as: E. M. de Medeiros, H. Noorman, R. Maciel Filho et al., Production of ethanol fuel via syngas fermentation: Optimization of economic performance and energy efficiency, Chemical Engineering Science: X, https://doi.org/10.1016/j.cesx.2020.100056

MOGA was chosen due to its robustness and easy implementation using the *gamultiobj* function in MATLAB R2015b, which employs a variant of the NSGA-II method (non-dominated sorting genetic algorithm).

For the standalone BCR, a population of 100 individuals was considered, while for the whole process populations ranging from 250 to 1000 were tested at multiple runs.

The objectives were always defined as minimization functions, hence in the first case (standalone BCR), the two objectives were: $OF_1 = -productivity = -D_{rate} \cdot C_{L,EtOH}$ and $OF_2 = CAPEX_{BCR}$. In the second case (whole process), two pairs of objectives were evaluated: (i) $OF_1 = CAPEX/\dot{m}_{AE}$, $OF_2 = -\eta$; and (ii) $OF_1 = MESP$, $OF_2 = -\eta$. All the optimizations were performed for two case studies regarding mass transfer capacity: a base case and a high mass transfer case (HMT) in which the k_La calculated with Eq. (6) was multiplied by a factor of 3, representing thus a hypothetical case where process intensification methods are employed to increase mass transfer (this is further discussed in Section 3.3). A summary of the steps required to compute the objective functions is given next, along with the definition of the decision variables (DVs) (note that for the standalone BCR, the procedure stops after the 1st step):

1. DVs related to the BCR (D_{rate}, *GRT*, *GRR*, *XP*, *L*, V_R) and fixed inputs (e.g. gas composition) are provided to the BCR model, which employs ANNs to calculate multiple responses (broth composition, gas conversions, cooling requirements). The design variables and some of the responses are also used to calculate economic variables (investment, cost of raw materials and utilities), as explained in Section 2.5.1. Pure water is considered as initial guess for the liquid feed of the bioreactor (this is later adjusted as explained in step 4). Power consumption and cooling requirements associated with the gas compressor (C-01) are also calculated in this step.
2. Applicable responses from step 1 (e.g. broth composition), DVs related to T-01 (*S:F*) and fixed inputs are provided to the ANNs that calculate the outputs of T-01 (compositions of the streams, reboiler and condenser duties, column diameter). Similarly, some of the outputs (e.g. reboiler duty) and inputs (e.g. number of stages) are used to calculate economic responses.
3. Applicable responses from step 2, DVs related to T-02 (N_{ST}, $F_{ST,V}$, $F_{ST,L}$ and *RR*) and fixed inputs are provided to the model of T-02. In this step, the distillate to feed ratio (*D:F*) in T-02 is determined through a minor optimization routine to guarantee an ethanol mass fraction of 0.925 in the distillate. The ANNs are employed again with the complete input vector (including *D:F*) to generate the relevant responses; other outputs and inputs are used to compute economic results, and heating/cooling requirements are also calculated for the adsorption unit.
4. With the outputs from steps 2 and 3, the composition of the liquid recycle stream is calculated and compared with the initial guess. If required, an iterative procedure is followed to match both streams.
5. If the ethanol mass fraction in the distillate from T-02 is 0.925 and other requirements are met (no negative mass flows, ANN inputs inside their training ranges, equipment capacities inside feasible ranges), then the outputs from steps 1–4 are combined to generate the objective functions, as further explained in Sections 2.5.1 and 2.5.2.

2.5.1. Computation of economic performance

Economic performance was evaluated in terms of total capital investment (*CAPEX*) and minimum ethanol selling price (*MESP*). The total investment was estimated using the module costing technique described by Turton et al. (2009), in which all the costs derive from the individual purchase cost of equipment at base conditions (C_p^0), estimated for each equipment of capacity *A* using Eq. (10). The total module cost (C_{TM}), which considers total direct and indirect costs, as well as contingencies and fees, is calculated as shown in Eq. (11). In the present work, *CAPEX* is considered the same as C_{TM}. The bare module cost of equipment *i*, $C_{BM,i}$, is calculated from $C_{p,i}^0$ applying bare module cost factors $F_{BM,i}$ which account for pressure, materials and other items such as installation and engineering. The coefficients K_1 and K_2 and the procedures to calculate F_{BM} for each type of equipment can be consulted in Turton et al. (2009).

$$\log_{10} C_p^0 = K_1 + K_2 \log_{10}(A) + K_2 [\log_{10}(A)]^2 \tag{10}$$

$$C_{TM} = 1.18 \cdot \sum_i C_{BM,i}, \quad C_{BM,i} = C_{p,i}^0 \cdot F_{BM,i} \tag{11}$$

The manufacturing costs COM_d (also called operating expenses or *OPEX*) comprise direct costs (e.g. raw materials [C_{RM}], utilities [C_{UT}], waste treatment [C_{WT}], maintenance, operating labor [C_{OL}]), fixed costs (e.g. overhead, depreciation, insurance) and general expenses (e.g. administration, R&D). The different components of the manufacturing costs can be estimated using multiplication factors based on historical data; adding up all these costs leads to an expression such as Eq. (12), used in the present work, which considers midpoint values from the ranges reported in Turton et al. (2009).

$$COM_d = 0.18 \cdot C_{TM} + 2.73 \cdot C_{OL} + 1.23 \cdot (C_{UT} + C_{WT} + C_{RM}) \tag{12}$$

The purchase price of syngas was considered 1 US$/kmol for the optimization runs, but its impact on *MESP* was later evaluated along with other economic parameters. The assumption was based on the ranges estimated with techno-economic modeling studies performed by Yao et al. (2018) and Martinez-Gomez et al. (2017) for syngas production from biomass and shale gas. Fuel for steam generation was considered to be sugarcane bagasse in Brazil, assuming a price of 2 US$/GJ which is inside the reported range from the last years (CanaOnline, 2016). The costs of utilities and waste treatment/disposal were calculated according to the methodology of Ulrich and Vasudevan (2006), also assuming an electricity price in accordance with the Brazilian context, at 0.12 US$/kWh (CPFL Energia, 2019). The cost of operating labor (C_{OL}) was assumed to be 3% of CAPEX.

With CAPEX (C_{TM}) and *OPEX*, the discounted cash flows can be calculated and the minimum ethanol selling price (*MESP*) can be found with a subordinate optimization routine to achieve *NPV* = 0, where *NPV* (Net Present Value) is the cumulative discounted cash flow at the end of the project. For this calculation a few considerations were made: (i) 15 years of project life and 2 years of construction; (ii) land cost = 7.5% C_{TM}; (iii) taxation rate = 35%; (iv) interest rate = 10%; (v) straight-line depreciation; (vi) project salvage value = 0; (vii) Chemical Engineering Plant Cost Index (CEPCI) = 615.9 as of December 2018 and CEPCI = 397 in base year (2001) (Chemical Engineering Magazine, 2019); and (viii) 350 days of operation per year.

2.5.2. Computation of thermodynamic performance

The thermodynamic performance was evaluated with the energy efficiency (η) as calculated in Eq. (13). The energy output is given by the lower heating value of ethanol fuel (LHV_{AE} = 26.5 MJ·kg^{-1}) multiplied by its production rate, and the total energy input is given by the *LHV* of syngas containing 50% CO and 50% H_2 (LHV_{syngas} = 252.4 MJ·kmol^{-1}) plus heat provided by steam at multiple parts of the process and the equivalent heat associated with the production of electricity consumed in compressors and pumps. For the latter, work-related energy was translated to heat

Please cite this article as: E. M. de Medeiros, H. Noorman, R. Maciel Filho et al., Production of ethanol fuel via syngas fermentation: Optimization of economic performance and energy efficiency, Chemical Engineering Science: X, https://doi.org/10.1016/j.cesx.2020.100056

by applying an electric generation efficiency of η_{CC} = 60% for combined cycles operating with natural gas (Siemens AG, 2019).

$$\eta = \frac{LHV_{AE} \cdot \dot{m}_{AE}}{LHV_{syngas} \cdot \dot{m}_{syngas} + \dot{E}_{in}} \quad , \quad \dot{E}_{in} = \sum \Delta \hat{H}_v \cdot \dot{m}_{steam} + \sum \dot{W}_{in}/\eta_{CC} \tag{13}$$

3. Results and discussion

3.1. Techno-economic optimization of the bubble column reactor (BCR)

Fig. 2 presents the main results of the optimization conducted for maximization of ethanol productivity and minimization of capital cost considering the standalone BCR. The goal of this study was to analyze the trends in Pareto-optimal points before connecting the BCR to the purification unit. Firstly, there is a clear trade-off between the two objectives, as shown with the Pareto fronts depicted in Fig. 2a for both case studies (normal and high mass transfer – HMT), meaning that, as expected, higher productivities can be achieved at the cost of higher investments. The Pareto fronts also seem to comprise at least two convex sub-sets of solutions. For example, for the base case, one subset lies in the region with productivities ≤3.15, after which there is a clear change of pattern in the Pareto front, which nonetheless continues to be convex. It's worth recalling that the 1st objective function is the minimization of *–productivity*, so it is not the objective function itself that is plotted in the x-axis, but its opposite value. For both cases there is a threshold after which the capital costs continue to increase without significant improvement in the productivity (e.g. after 4.5 $g{\cdot}L^{-1}{\cdot}h^{-1}$ for the base case, as seen in Fig. 2a). These optimal solutions are associated with larger reactor volumes (hence higher capital costs) obtained by decreasing the vessel aspect ratio (the length remains constant, as seen in Fig. 2c); but since the gains in productivity are only marginal, these are solutions without interest to the decision-making process. It is also verified that

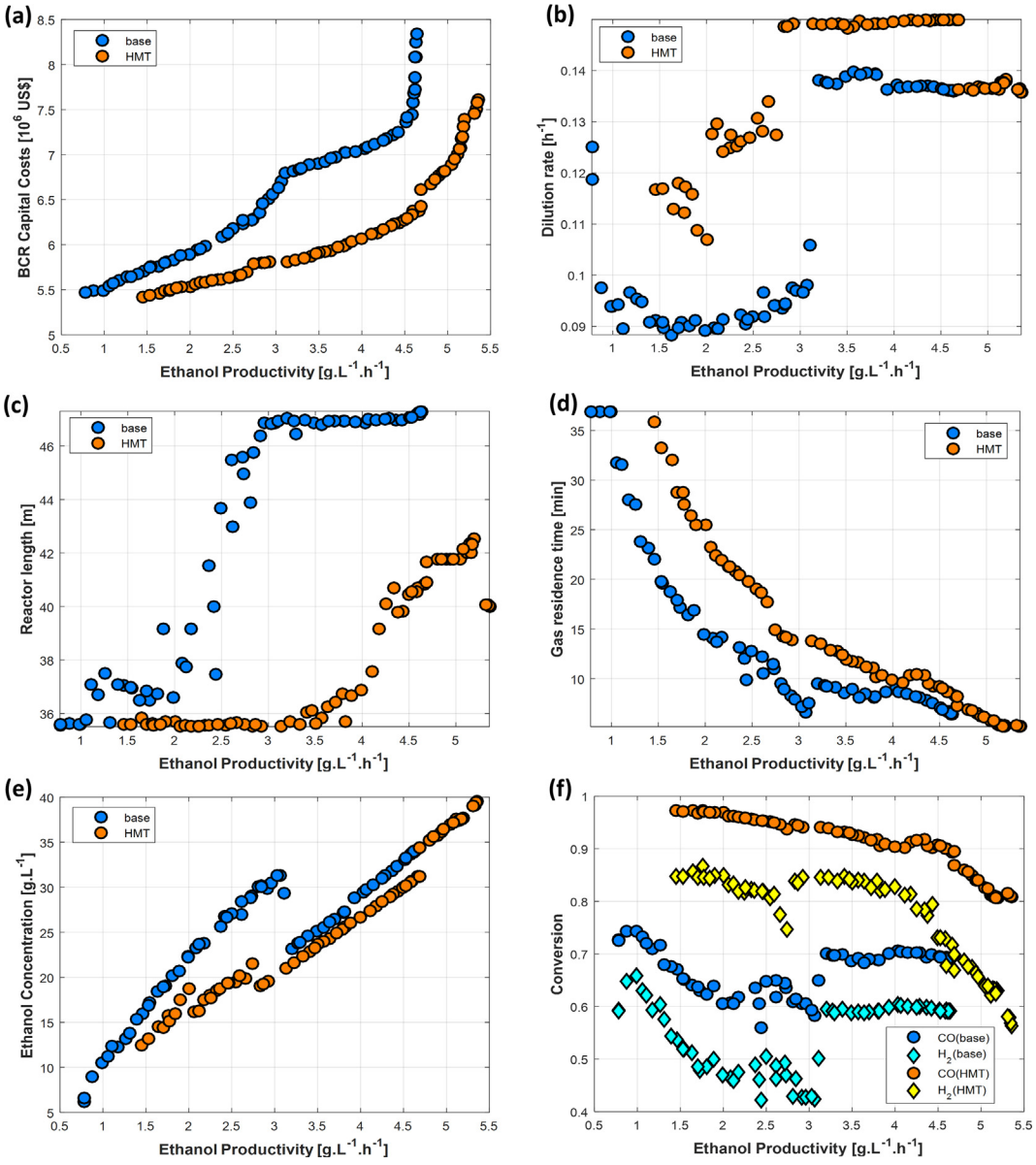

Fig. 2. Bi-objective optimization of the BCR for maximization of ethanol productivity and minimization of capital costs: Pareto fronts (a); selected decision variables at the Pareto-optimal solutions (dilution rate (b), reactor length (c), and gas residence time (d)); selected process outcomes at the Pareto-optimal solutions (ethanol concentration (e), gas conversions (f)).

Please cite this article as: E. M. de Medeiros, H. Noorman, R. Maciel Filho et al., Production of ethanol fuel via syngas fermentation: Optimization of economic performance and energy efficiency, Chemical Engineering Science: X, https://doi.org/10.1016/j.cesx.2020.100056

increasing the mass transfer coefficient leads to higher productivities with the same investment, at some points being almost twice the value of the base case.

The different Pareto subsets are produced by different combinations of the decision variables, as shown in Fig. 2b–d. Both case studies show one subset of solutions characterized by large and nearly constant values of dilution rate and reactor length. In this subset, the productivity continues to increase due to decreasing *GRT* (Fig. 2d) and increasing gas recycle ratio (not shown). In the preceding subset, the increase in productivity is not only due to decreasing *GRT* but also to increasing reactor length, in combination with changes in D_{rate} and *GRR*. These variations, of course, also have effects on the capital costs (as seen in Fig. 2a): for example, increasing the reactor length has a direct effect on the bioreactor cost; on the other hand, decreasing *GRT* implies increasing the gas flow rate, which brings higher costs associated with larger gas compressor capacities.

As presented in Table 1, the decision variables at the optimal solutions are constrained to similar ranges for both study cases (e.g. optimal vessel volumes are close to the lower bound of the stipulated search space), but the process outcomes are mostly improved when mass transfer is enhanced. Higher conversions are achieved for both CO and H_2 (shown in Fig. 2f), as well as higher ethanol concentrations (Fig. 2e), though in this case the HMT results also show lower concentrations for a wide range of productivities.

3.2. Thermo-economic optimization of the integrated process

Integrating the BCR to the purification unit brought several difficulties due to the high non-linearity of the MESH equations, which often leads to infeasible solutions, and the inclusion of a recycle stream of distillate bottoms containing traces of ethanol and acetic acid. This was observed by the much longer time required to run the optimization (from 5 min to over 3 h), despite the use of reduced (surrogate) models. Another reason for the higher complexity of the integrated model is that the input variables of the distillation columns must be set to guarantee an ethanol mass fraction of 0.925 in the distillate stream of the second column.

The generated Pareto fronts are depicted in Fig. 3, where again the opposite of an objective function is shown: for all fronts in Fig. 3, the 2nd objective function was to minimize $-\eta$, but η itself is plotted in the y-axis. As explained in Section 2.5, the optimization was performed for two mass transfer cases (base and HMT) and two pairs of objective functions. The difference between these pairs is the formulation of the 1st objective function, which is either to minimize $CAPEX/\dot{m}_{AE}$ (Fig. 3a–b) or *MESP* (Fig. 3c–d). It's worth mentioning that the results presented here are the best found approximations of the Pareto fronts, which were selected after multiple runs of the multi-objective genetic algorithm.

The first observation is that the thermodynamic efficiency was bounded to around 0.42 in the base model and 0.72 in the HMT case, also with lower *CAPEX* and *MESP* achieved in the latter. The trade-off is visible for all cases, although the optimization of the η-MESP pair with HMT (Fig. 3d) led to a small set of non-dominated solutions distributed between $0.707 \leq MESP$ (US$/L) ≤ 0.713. As explained by Goh and Tan (2009), finding a diverse set of solutions is specially challenging in the presence of multimodality (i.e. multiple local Pareto fronts), discontinuity and non-uniformity. Moreover, balancing diversity of solutions and proximity to the true Pareto front is a multi-objective problem in itself, since these two qualities are both desirable and conflicting (Bosman and Thierens, 2003). Despite the lack of diversity in the solutions presented in Fig. 3d, the results are deemed sufficient for the purposes of the present work, and testing different algorithms to improve this aspect is left as recommendation for a future work.

To support the interpretation of the Pareto fronts, the Pareto-optimal values of two selected decision variables are shown in Fig. 4 along with process outcomes. In this figure, optimization A (Opt_A, circles) refers to the objective pair *(CAPEX,η)* and B (Opt_B, diamonds) to the pair *(MESP,η)*. For both mass transfer cases, the increase in η (accompanied by increase in *CAPEX* and *MESP*) was associated with a decrease in D_{rate} (Fig. 4a) and increase in *GRT* (Fig. 4b), though in the HMT case the range spanned by these variables was very narrow. Other DVs (not shown here) that had predominant increasing trends with η were the gas recycle ratio (*GRR*), the number of stages in T-02 and its reflux ratio. Fig. 4 also suggests that in the base case the Opt_B Pareto front (*MESPxη*) constitutes a subset of Opt_A (*CAPEXxη*), with decision variables and process outcomes following similar trends and ranges. This also happens to a lesser extent with HMT.

The minimum and maximum values of the optimal DVs are presented in Table 2, where it can be observed that for all case studies and optimization pairs the ranges were significantly reduced from the search space. For comparison, the ranges obtained by minimizing *MESP* as a single objective are also shown. The minimum values of *MESP* in this case were 0.958 US$/L (base) and 0.705 US$/L (HMT), but the energy efficiencies at these points were far from their highest values, at 0.31 and 0.50 respectively, indicating that inefficiencies are compensated by low price of resources. An intriguing outcome is that when optimizing a single objective many DVs had optimal values outside the ranges of the Pareto-optimal solutions; in fact, this was observed for all the DVs in the HMT case. For the gas recycle ratio (GRR) specially, the single-objective optimum was close to zero while being almost at the search space upper bound for Pareto-optimal points with higher η.

This illustrates the importance of using multi-objective as opposed to single-objective optimization: as technology progress is driven by multiple values other than economic profit, it is inevitable that industries will seek to optimize conflicting objectives; and not only bi-objective but many-objective problems will need to be tackled. In fact, even if the goals are kept within the economic sphere, it is still challenging to reduce them to a single variable, since different indicators can be used to evaluate the profitability of a process: *CAPEX*, *MESP*, *OPEX*, *NPV*, payback time, *ROI* (return on investment), etc.

It's worth noting that the optimization of the BCR alone is not enough for meaningful decision-making, since the operating and design variables of the purification unit must be adapted to the outcomes of the bioreactor and optimized accordingly. When analyzing the whole process, the possible choices for the operating conditions and design variables were optimized to give a range of solutions from which a single one can be picked. If both energy efficiency and MESP are considered equally important, an illustrative example for the base case is to take the solution at $\eta \approx 0.4$ following the notably steep increase in Fig. 3c, since after this point the gains in efficiency are relatively slow with respect to MESP. This solution gives the following decision variables: $D_{rate} = 0.052\ h^{-1}$, *GRT* = 34.1 min, *GRR* = 0.37, *XP* = 0.13, *L* = 49.5 m, V_R = 772 m^3, *S:F* = 0.10, N_{ST} = 45, $F_{ST,V}$ = 0.65, $F_{ST,L}$ = 0.4, and *RR* = 5.55. For the high mass transfer case, a similar solution can be drawn out at $\eta \approx 0.714$: $D_{rate} = 0.10\ h^{-1}$, *GRT* = 18.6 min, *GRR* = 0.49, *XP* = 0.05, *L* = 42.7 m, V_R = 652 m^3, *S:F* = 0.08, N_{ST} = 44, $F_{ST,V}$ = 0.76, $F_{ST,L}$ = 0.34, and *RR* = 3.95.

Relevant process outcomes are presented in Table 3. The average ethanol concentration in the broth was around 29 $g{\cdot}L^{-1}$ for the base case and 36 $g{\cdot}L^{-1}$ for the HMT case, with the acetic acid concentration staying under 4 $g{\cdot}L^{-1}$. As consequence, lower energy consumption in the distillation unit (roughly 7.2 MJ/L ethanol)

Please cite this article as: E. M. de Medeiros, H. Noorman, R. Maciel Filho et al., Production of ethanol fuel via syngas fermentation: Optimization of economic performance and energy efficiency, Chemical Engineering Science: X, https://doi.org/10.1016/j.cesx.2020.100056

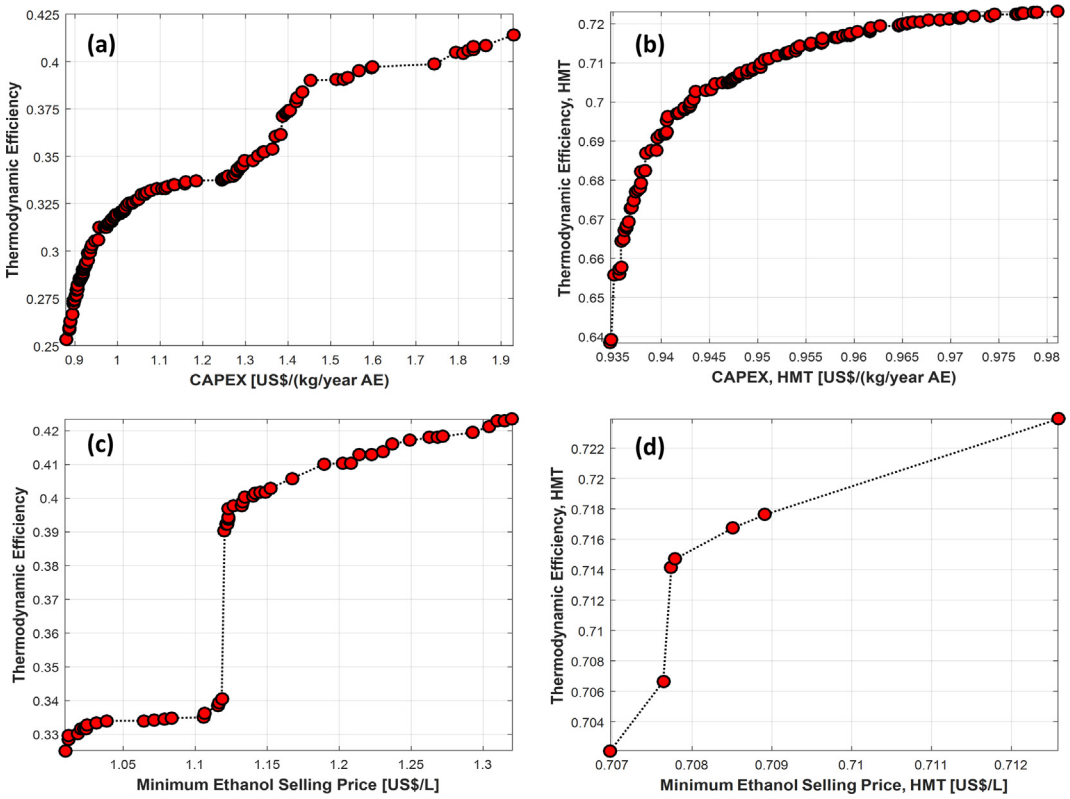

Fig. 3. Bi-objective optimization of the integrated units: optimization A with base (a) and high mass transfer model (b); optimization B with base (c) and high mass transfer model (d).

could be obtained with HMT, while the base case spans a range from 7.4 to 9.4 MJ/L, mostly increasing with η. The results also show that high CO conversions (Fig. 4c) of up to 97% can be achieved with increased mass transfer and 83% for the base case, while the H_2 conversions (Fig. 4d) were bounded to lower values (74%) in both cases, due to the CO inhibition as considered in the kinetic model. For comparison purposes, LanzaTech's process is able to achieve high and stable CO conversions above 90% and ethanol selectivity of 95% (LanzaTech, 2018). Though their process configuration might be similar to the one considered here, employing gas-liquid column reactors, distillation to purify ethanol, and water recycle, the exact design and conditions of their process are not reported. Another point worth mentioning is that in the present work the gas composition was fixed at 50% CO and 50% H_2, but the proportions of $CO/H_2/CO_2$ are also expected to have significant impacts on the gas conversion and ethanol productivity in the bioreactor (de Medeiros et al., 2019). Since the syngas composition is a result of design choices in upstream stages, which in turn also affect prices and energy efficiency, another study is currently under development for the impact analysis and optimization of the whole process including syngas production via gasification.

The Pareto-optimal solutions of the integrated process span smaller ranges of ethanol productivity in the bioreactor than the BCR optimization, indicating that higher productivities are not necessarily advantageous when taking into account the whole process, due to much higher capital costs (also corroborated by the steep increase in the Pareto fronts from Fig. 2a) and losses in gas conversion (thus lower energy efficiency). With regard to the annual production of anhydrous ethanol (Fig. 4e), in the base case the trends are opposite to the energy efficiency, but with HMT there doesn't seem to be a correlation between the two, with the optimal production rate in this case being between 121 and 133 MML/year. However, if *MESP* is used as single objective both cases lead to similar production rates of around 121–124 MML/year (Table 3).

3.3. Effects and prospects of mass transfer enhancement

It can also be observed in Fig. 4 and Table 2 that the optimal values of the decision variables differ significantly between the base case and the HMT case, demonstrating the importance of accurate k_La estimations for the effective application of model-based optimization results. Several factors could compel the real k_La to deviate from the predictions of empirical correlations such as Eq. (6), for example the presence of salts and alcohols in low concentration, which have been shown to increase k_La by factors up to 2 (van de Donk, 1981). Heijnen and van't Riet (1984) have also noted that, in non-coalescing media, fine bubble systems can present a six-fold increase in k_La as compared to coarse bubble systems measured at the same gas superficial velocity, although in strongly coalescing media the difference is modest. Therefore the results presented here suggest that great improvements can be achieved with ingenious tuning of k_La via enhancement techniques. Ultimately, such "mass transfer enhancement" can be included as a factor in the optimization framework in order to find the optimal amount of efforts and costs that should be spent into increasing mass transfer capacity in the bioreactor. Examples of process intensification (PI) strategies for this purpose are given next.

Groen et al. (2005) presented a method to increase the oxygen transfer capacity in aerobic fermentation which consisted of injecting a second gas stream (pure oxygen) via a special nozzle configuration to achieve supersonic velocities and a non-uniform bubble size distribution. With a ratio of 6:1 between the two gas flows (air/pure oxygen) the authors were able to increase the mass transfer rate 3.6 times. Along the lines of reducing bubble size to increase the surface to volume ratio, the generation of micron size (<1 mm) bubbles is generally considered an efficient way of enhancing gas-liquid mass transfer while requiring low power inputs: Bredwell and Worden (1998), for example, obtained a six-times higher k_La using a spinning-disk microbubble generator

Please cite this article as: E. M. de Medeiros, H. Noorman, R. Maciel Filho et al., Production of ethanol fuel via syngas fermentation: Optimization of economic performance and energy efficiency, Chemical Engineering Science: X, https://doi.org/10.1016/j.cesx.2020.100056

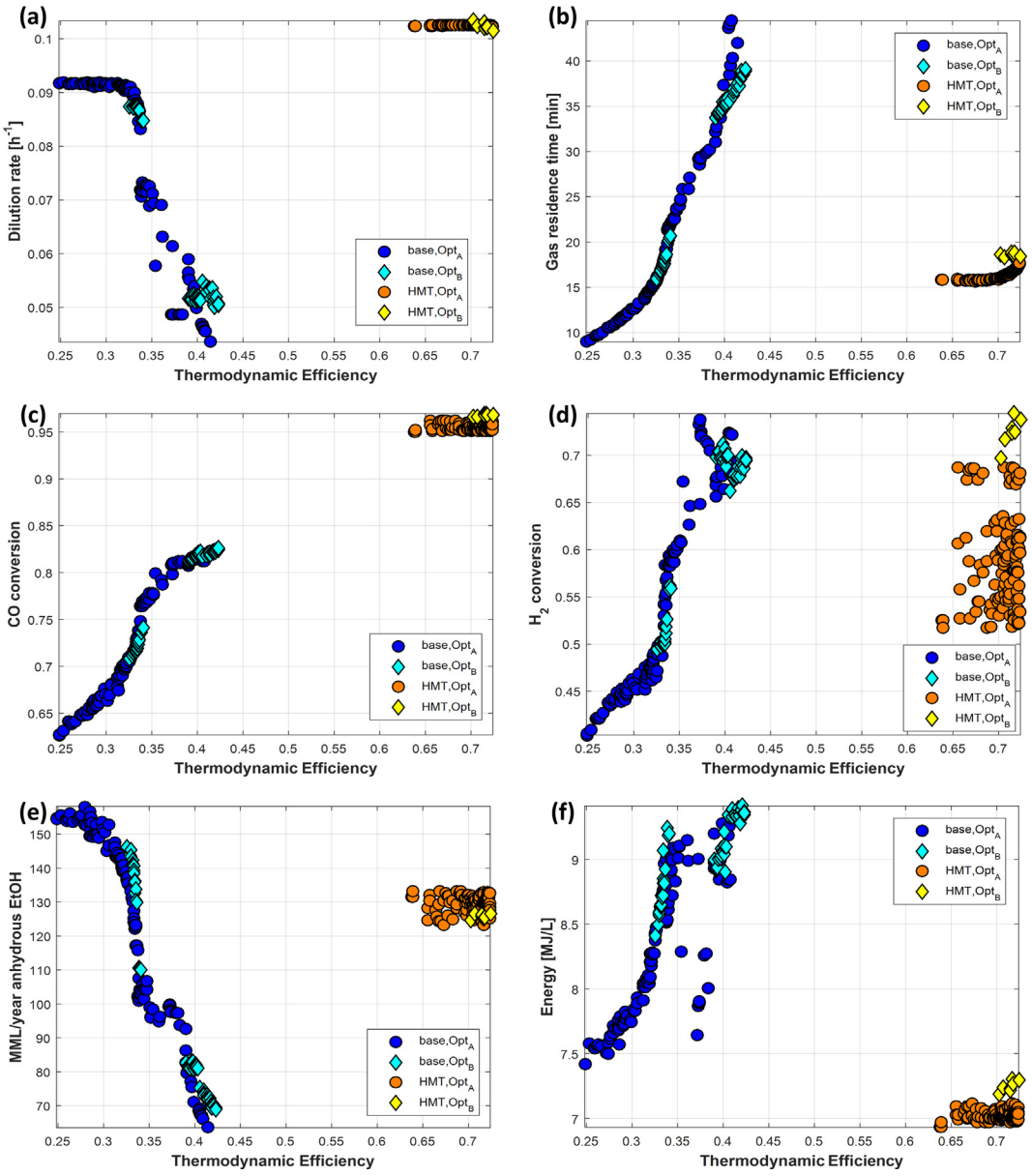

Fig. 4. Bi-objective optimization of the integrated units: selected decision variables at the Pareto-optimal solutions (dilution rate (a) and gas residence time (b)); selected process outcomes at the Pareto-optimal solutions (CO conversion (c), H_2 conversion (d), production rate (e), and energy consumption (f)).

Table 3
Multi-objective optimization of the integrated process: ranges of process outcomes at the Pareto-optimal solutions.

	CAPEX × η	CAPEX × η (HMT)	MESP × η	MESP × η (HMT)	MESP	MESP (HMT)
$C_{L,EtOH}$ (BCR) [g·L^{-1}]	26.3–34.7	36.6–38.3	26.0–30.1	35.5–36.7	28.4	34.6
$C_{L,HAc}$ (BCR) [g·L^{-1}]	1.61–3.74	2.33–2.43	1.97–3.44	2.33–2.46	4.20	3.0
Heat consumption [MJ·L^{-1} AE]	7.42–9.35	6.93–7.11	8.41–9.41	7.18–7.30	8.71	7.45
Electricity consumption [kWh·L^{-1} AE]	0.40–0.58	0.37–0.41	0.40–0.53	0.36–0.37	0.43	0.25
X_{CO}(BCR)	0.63–0.82	0.95–0.96	0.71–0.83	0.97	0.68	0.97
X_{H_2}(BCR)	0.40–0.74	0.52–0.69	0.50–0.71	0.70–0.74	0.40	0.78
$\dot{m}_{AE}$ [MML·year^{-1}]	63.5–158	123–133	68.8–146	125–127	124	121
EtOH Productivity (BCR) [g·L^{-1}·h^{-1}]	1.17–3.19	3.74–3.93	1.33–2.63	3.66–3.73	2.81	3.67

as compared to the conventional sparging system in a stirred tank for syngas fermentation. Moreover, while micro-porous diffusers can be used to generate microbubbles in a passing gas stream, several works have demonstrated even further size reduction by oscillating this stream, with the oscillation frequency in this case being a central optimization variable (Brittle et al., 2015). A myriad of other methods have also been reported for the formation of microbubbles, relying on different aspects: with or without accompanying liquid flows, using polymers or with very low power consumption such as microchannel techniques and ultrasonic systems (Parmar and Majumder, 2013).

Finally, nanoparticles have also been shown to improve mass transfer, though only limited work has been developed for syngas fermentation. Kim and Lee (2016), for example, observed substan-

Please cite this article as: E. M. de Medeiros, H. Noorman, R. Maciel Filho et al., Production of ethanol fuel via syngas fermentation: Optimization of economic performance and energy efficiency, Chemical Engineering Science: X, https://doi.org/10.1016/j.cesx.2020.100056

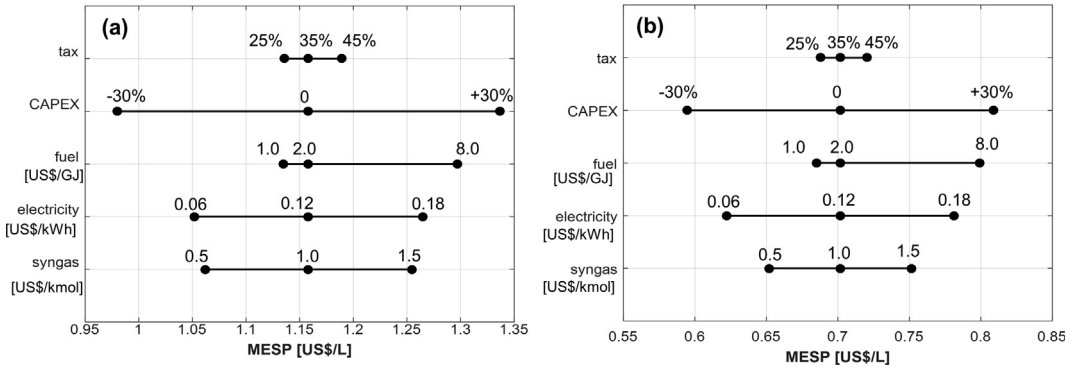

Fig. 5. Sensitivity of MESP to economic parameters: base (a) and high mass transfer model (b).

tial increase in the dissolved concentrations of CO, H_2 and CO_2 when using functionalized nanoparticles, and they also reported that adding a magnetic layer to the particles enabled their reuse up to five times, thereby improving their economic feasibility.

3.4. Sensitivity of MESP

The Pareto-optimal *MESP* was in the range 1.0–1.3 US$/L (base) and 0.707–0.713 US$/L (HMT), while in a previous work by our group the estimated *MESP* for a process including biomass gasification and heat/power generation was in the range 0.63–0.93 US$/L hydrous ethanol (i.e. before dehydration) (de Medeiros et al., 2017). In another study about syngas fermentation, even higher values between 1.58 and 1.93 US$/L were found (Benalcázar et al., 2017). Not only technical considerations and process modeling methods lead to these disparities, but also economic considerations such as the prices of utilities and raw materials. With that in mind, Fig. 5 shows the sensitivity of *MESP* to several economic parameters, where the midpoint is one of the Pareto-optimal solutions from Fig. 3c and 3d. In this analysis the parameters were varied each at a time, with the other parameters being fixed at the values used in the optimization. For both cases the highest impacts on *MESP* (around 15% of its original value) were caused by a 30% change in the capital investment, which might also explain why the optimizations with *CAPEX* and *MESP* have similar results. A forthcoming work by our group suggests that in other cases *MESP* can decrease with higher η, probably because the contributions of raw materials and utilities are more significant than in the present study.

4. Conclusions

Different process systems engineering (PSE) tools (modeling, simulation, neural networks, genetic algorithm) were applied in this work to develop an optimization framework through which ranges of operating conditions and design variables can be selected for optimal production of ethanol fuel from syngas via fermentation, taking into account objectives of distinct natures. When optimizing a standalone bioreactor (BCR) in terms of ethanol productivity and capital costs, it was observed that Pareto-optimal values of productivity ranged between 0.75–4.5 $g{\cdot}L{\cdot}h^{-1}$ for the base model and 1.5–5.4 $g{\cdot}L^{1}{\cdot}h^{-1}$ for an optimistic case with higher mass transfer capacity (HMT), with the productivity increasing at the cost of higher investment due to larger reactor vessel and gas compressor. In the second part of this work, the BCR model was coupled to the purification unit including water recycle, and the integrated process was optimized in terms of economic variables (*CAPEX* and *MESP*) and energy efficiency (η). It was observed that, with the assumptions used here, *MESP* and *CAPEX* increase with η, which nonetheless was restricted to maximum values of 0.42 (base case) and 0.72 (HMT). The trends of the decision variables along the Pareto fronts were discussed and it was seen that optimization results are greatly affected by the mass transfer calculations, thus corroborating that k_La enhancement is a promising strategy for global process improvement. The results presented here provide information about key process conditions and design variables, as well as sustainability targets and limitations in syngas fermentation. This work can be further extended to evaluate and optimize the whole process from biomass waste to ethanol or other chemicals, and its reliability can be increased with the development of new models for syngas fermentation.

CRediT authorship contribution statement

Elisa M. de Medeiros: Conceptualization, Methodology, Software, Formal analysis, Investigation, Writing - original draft, Writing - review & editing, Visualization. **Henk Noorman:** Conceptualization, Resources, Writing - review & editing, Supervision, Funding acquisition. **Rubens Maciel Filho:** Conceptualization, Resources, Supervision. **John A. Posada:** Conceptualization, Resources, Writing - review & editing, Supervision.

Declaration of Competing Interest

The authors declare that they have no known competing financial interests or personal relationships that could have appeared to influence the work reported in this paper.

Acknowledgments

The authors thank DSM (Netherlands) and BE-Basic Foundation for the financial support provided in the form of a Ph.D. scholarship for E. M. de Medeiros. The research was also supported by São Paulo Research Foundation (FAPESP-Brazil), grant #2015/20630-4. This work is part of a Dual Degree Ph.D. project under the agreement between UNICAMP (Brazil) and TU-Delft (Netherlands).

References

Abubackar, H.N., Veiga, M.C., Kennes, C., 2015. Carbon monoxide fermentation to ethanol by *Clostridium autoethanogenum* in a bioreactor with no accumulation of acetic acid. Bioresour. Technol. 186, 122–127.

ArcelorMittal, 2019. World first: ArcelorMittal Belgium starts construction on two pioneering projects to further reduce carbon emissions. https://belgium.arcelormittal.com/en/two-pioneering-projects-to-further-reduce-carbon-emissions/ (accessed 22-07-2019).

Benalcázar, E.A., Deynoot, B.G., Noorman, H., Osseweijer, P., Posada, J.A., 2017. Production of bulk chemicals from lignocellulosic biomass via thermochemical conversion and syngas fermentation: a comparative techno-economic and environmental assessment of different site-specific supply chain configurations. Biofuels. Bioprod. Bioref. 11, 861–886.

Biofuels Digest, 2019. South Africa gives green light to country's first LanzaTech ethanol project. http://www.biofuelsdigest.com/bdigest/2018/10/23/south-africa-gives-green-light-to-countrys-first-lanzatech-ethanol-project/ (accessed 22-07-2019).

Bosman, P.A.N., Thierens, D., 2003. The balance between proximity and diversity in multiobjective evolutionary algorithms. IEEE Trans. Evolut. Comput. 7 (2), 174–188.

Bredwell, M.D., Worden, R.M., 1998. Mass-transfer properties of microbubbles. 1. Experimental studies. Biotechnol. Prog. 14, 31–38.

Brittle, S., Desai, P., Ng, W.C., Dunbar, A., Howell, R., Tesař, V., Zimmerman, W.B., 2015. Minimising microbubble size through oscillation frequency control. Chem. Eng. Res. Des. 104, 357–366.

CanaOnline, 2016. Há um ano, bagaço de cana era vendido por R$150,00 a tonelada, agora chega a R$25,00. http://www.canaonline.com.br/conteudo/ha-um-ano-bagaco-de-cana-era-vendido-por-r15000-a-tonelada-agora-chega-a-r2500.html (accessed 19/03/2019).

Chemical Engineering Magazine, 2019. https://www.chemengonline.com/pci (accessed 20/03/2019).

Chen, J., Daniell, J., Griffin, D., Li, X., Henson, M.A., 2018. Experimental testing of a spatiotemporal metabolic model for carbon monoxide fermentation with *Clostridium autoethanogenum*. Biochem. Eng. J. 129 (2018), 64–73.

CPFL Energia, 2019. https://www.cpflempresas.com.br/institucional/tarifas.aspx?emp=CPFL (accessed 19/03/2019).

de Medeiros, E.M., Posada, J.A., Noorman, H., Osseweijer, P., Filho, R.M., 2017. Hydrous bioethanol production from sugarcane bagasse via energy self-sufficient gasification-fermentation hybrid route: simulation and financial analysis. J. Clean. Prod. 168, 1625–1635.

de Medeiros, E.M., Posada, J.A., Noorman, H., Filho, R.M., 2019. Dynamic modeling of syngas fermentation in a continuous stirred-tank reactor: multi-response parameter estimation and process optimization. Biotechnol. Bioeng. 2019, 1–15. https://doi.org/10.1002/bit.27108.

Deckwer, W.-D., 1976. Non-isobaric bubble columns with variable gas velocity. Chem. Eng. Sci. 31, 309–317.

Deckwer, W.-D., 1992. Bubble Column Reactors (V. Cottrell, Trans.). John Wiley & Sons Ltd, Chichester.

Deckwer, W.-D., Burckhart, R., Zoll, G., 1974. Mixing and mass transfer in tall bubble columns. Chem. Eng. Sci. 29, 2177–2188.

Goh, C.-K., Tan, K.C., 2009. Evolutionary Multi-objective Optimization in Uncertain Environments: Issues and Algorithms. Springer-Verlag, Berlin Heidelberg.

Goldemberg, J., Coelho, S.T., Guardabassi, P., 2008. The sustainability of ethanol production from sugarcane. Energy Policy 36, 2086–2097.

Groen, D.J., Noorman, H.J., Stankiewicz, A., 2005. Improved method for aerobic fermentation intensification. In: Jansens, P.J., Stankiewicz, A., Green, A. (Eds.), Proceedings of Sustainable (Bio)Chemical Process Technology Incorporating 6th Int. Conf. Process Intensification. BHR Group Ltd., Cranfield, pp. 105–112.

Heijnen, J.J., Vant Riet, K., 1984. Mass transfer, mixing and heat transfer phenomena in low viscosity bubble column reactors. Chem. Eng. J. 28, B21–B42.

Humbird, D., Davis, R., Tao, L., Kinchin, C., Hsu, D., Aden, A., Schoen, P., Lukas, J., Olthof, B., Worley, M., Sexton, D., Dudgeon, D., 2011. Process design and economics for biochemical conversion of lignocellulosic biomass to ethanol: dilute-acid pretreatment and enzymatic hydrolysis of corn stover. Technical Report, NREL/TP-5100-47764 (May 2011).

Ibrahim, D., Jobson, M., Li, J., Guillén-Gosálbez, G., 2018. Optimization-based design of crude oil distillation units using surrogate column models and a support vector machine. Chem. Eng. Res. Des. 134, 212–225.

IEA, 2019. https://www.iea.org/statistics/co2emissions/ (accessed 26/06/2019).

Kim, Y.-K., Lee, H., 2016. Use of magnetic nanoparticles to enhance bioethanol production in syngas fermentation. Bioresour. Technol. 204, 139–144.

LanzaTech, 2018. LanzaTech – No such thing as waste. https://ccnet-nibb.co.uk/wp-content/uploads/2018/04/simpson.pdf (accessed 08/08/2019).

Li, X., Griffin, D., Li, X., Henson, M.A., 2019. Incorporating hydrodynamics into spatiotemporal metabolic models of bubble column gas fermentation. Biotechnol. Bioeng. 116, 28–40.

Martinez-Gomez, J., Nápoles-Rivera, F., Ponce-Ortega, J.M., El-Halwagi, M.M., 2017. Optimization of the production of syngas from shale gas with economic and safety considerations. Appl. Therm. Eng. 110, 678–685.

Pardo-Planas, O., Atiyeh, H.K., Phillips, J.R., Aichele, C.P., Mohammad, S., 2017. Process simulation of ethanol production from biomass gasification and syngas fermentation. Bioresour. Technol. 245, 925–932.

Parmar, R., Majumder, S.K., 2013. Microbubble generation and microbubble-aided transport process intensification – a state-of-the-art report. Chem. Eng. Process. 64, 79–97.

Renewables Now, 2018. LanzaTech, Shougang open sustainable ethanol refinery in China. https://renewablesnow.com/news/lanzatech-shougang-open-sustainable-ethanol-refinery-in-china-615844/ (accessed 22-07-2019).

Richter, H., Molitor, B., Wei, H., Chen, W., Aristilde, L., Angenent, L.T., 2016. Ethanol production in syngas-fermenting *Clostridium ljungdahlii* is controlled by thermodynamics rather than by enzyme expression. Energy Environ. Sci. 9, 2392–2399.

Roy, P., Dutta, A., Deen, B., 2015. Greenhouse gas emissions and production cost of ethanol produced from biosyngas fermentation process. Bioresour. Technol. 192, 185–191.

Siemens AG, 2019. Gas Turbine Portfolio Brochure. https://siemens.com/gasturbines (accessed 17-07-2019).

Turton, R., Bailie, R.C., Whithing, W.B., Shaeiwitz, J.A., 2009. Analysis, Synthesis, and Design of Chemical Processes. Prentice Hall, New Jersey.

Ulrich, G.D., Vasudevan, P.T., 2006. How to estimate utility costs. Chem. Eng. (April 2006), 66–69.

Van de Donk, J., 1981. Water Aeration with Plunging Jets PhD thesis. Delft University of Technology.

Yao, Z., You, S., Ge, T., Wang, C.-H., 2018. Biomass gasification for syngas and biochar co-production: energy application and economic evaluation. Appl. Energy 209, 43–55.

Ye, F., Ma, S., Tong, L., Xiao, J., Bénard, P., Chahine, R., 2019. Artificial neural network based optimization for hydrogen purification performance of pressure swing adsorption. Int. J. Hydrogen Energy 44, 5334–5344.

Please cite this article as: E. M. de Medeiros, H. Noorman, R. Maciel Filho et al., Production of ethanol fuel via syngas fermentation: Optimization of economic performance and energy efficiency, Chemical Engineering Science: X, https://doi.org/10.1016/j.cesx.2020.100056